Thermal Biophysics Lectures

Rajiv Chopra
chopra@sri.utoronto.ca
Rm C713, Imaging Research
Sunnybrook Health Sciences Centre
2075 Bayview Avenue, Toronto, Ontario, M4N3M5

Big Picture

- Lecture 1: Biology/Rationale/Nomenclature
- Lecture 2: Blood Flow/Modelling
- Lecture 3: Energy Delivery
- **Lecture 4: Thermometry/Treatment monitoring**

MONITORING & EVALUATION

Thermometry

1. Enables quantification of amount of heating delivered to target volume during treatment
    - Can calculate thermal dose

2. Enables quantification of amount of heating delivered to surrounding tissues during treatment
    - Safety thresholds

3. Provides real measurement of *in situ* energy deposition

4. Can be used to control the treatment to achieve a desired thermal profile

Thermometry Requirements

- Depends on the nature of heating (hyperthermia vs. high temperature thermal therapy)

	Hyperthermia *43-47°C, hours-minutes*	**High Temperature Thermal Therapy** *>55°C, minutes-seconds*
Spatial Resolution	3-10 mm	1-2 mm
Temporal Resolution	10-15 seconds	1-5 seconds
Temperature resolution	≤ 1 °C	2-3 °C
Range of measurement	<37 – 50 °C	<37 - >90 °C

Invasive Measurements

1. Thermocouples
   - Can be made very small (~50um)
   - MRI-compatible materials (copper-constantin)
   - Wide range, accurate, cheap
   - Can absorb energy during heating giving false readings

2. Fibre-optic sensors
   - Can be as small as ~500 um
   - MRI-compatible
   - Sufficient range, 0.2-0.5°C precision, $$
   - Can be affected by heating during photothermal therapy

- Still play an important role for validation/body temperature measurement during image-guided thermal therapy

Ultrasound Thermometry

Three main methods:

1. Speed of sound
2. Backscatter
3. Attenuation

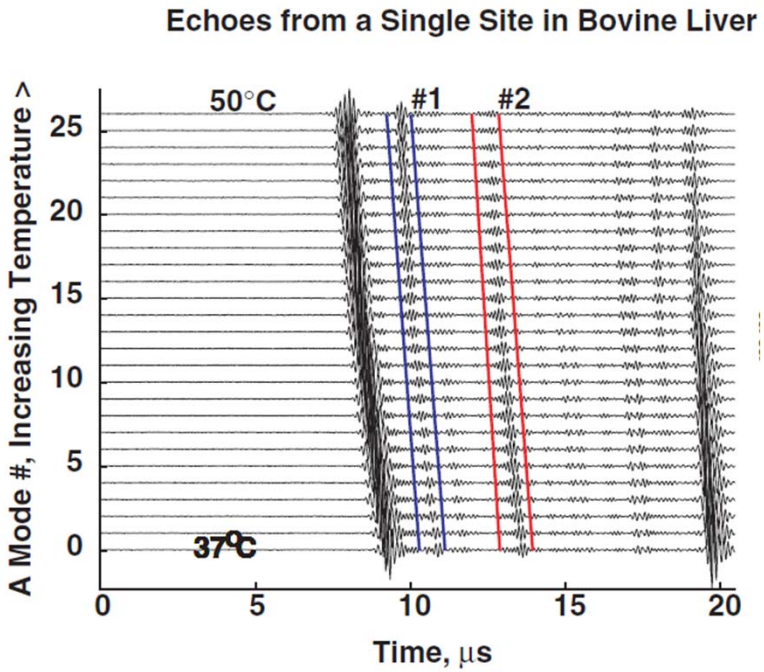

Figure 1. Changes in backscattered ultrasound with temperature. (Left) Echoes measured from a single site in a 1 cm thick sample of fresh bovine liver at temperatures from 37–50°C. The two delineated echoes (indicated by bands marked #1 and #2) shift with temperature have energies that appear to change with temperature (similar to Figure 4 in [29]). (Right) RF images of a fixed region in bovine liver showing apparent motion from 37–50°C. The right panel shows the image at 50°C after motion compensation.

- Major weakness of these methods are
  1. Small changes over temperature range
  2. Requirement for prior knowledge of tissue composition and temperature dependence

Ultrasound Thermometry

Speed of sound

- Manifested as apparent shifts of scatterers
- Temperature dependence of fat and tissue is different…requires a priori knowledge of tissue type
- Tissue thermal expansion is a competing effect that affects the same signal being measured…knowledge of this is required

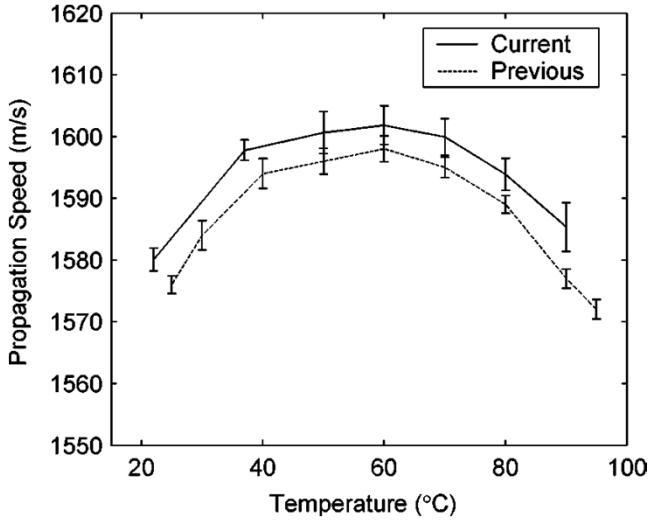

Canine Liver, Techavipoo et al

$$\Delta T(z) = c_0/2(\alpha - \beta) \times \delta t(z)/\delta z$$

α-linear coefficient of thermal expansion, β – change in c with temperature, co – speed of sound before heating, z – depth, t(z) – time shift at depth z,

Straube et al, IJH, 2005

Ultrasound Thermometry

Backscattered Energy

- Change in the received power as a function of temperature
- Due to the change in speed of sound between scatterers and the medium
- Depends on the medium type

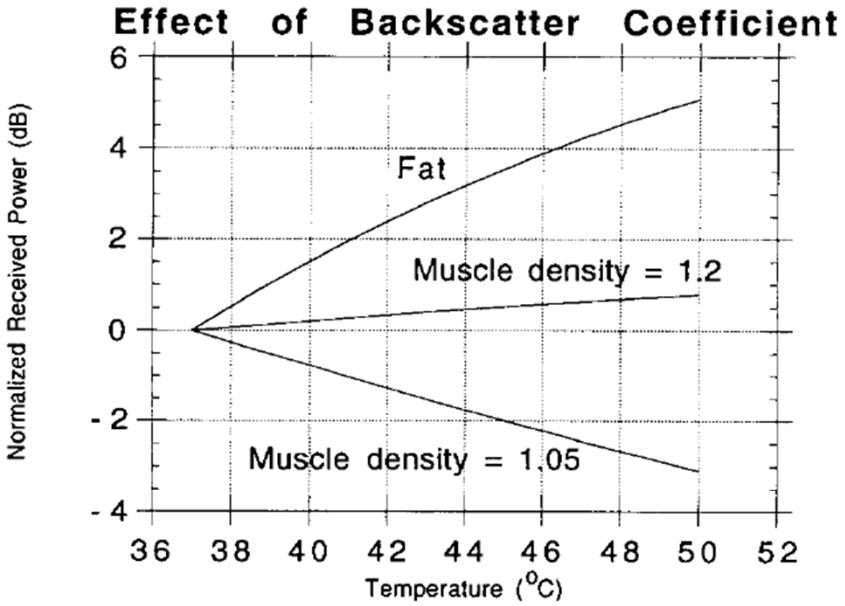

Fig. 5. The effect of the temperature dependence of the backscatter coefficient on the normalized backscattered power. The curves plotted are the result of evaluating eqn (2) using the polynomial shown in Figs. 2 and 3 for the temperature dependence of velocity to calculate the backscatter coefficient using eqn (4). Attenuation was fixed. The curve labeled Fat was the result of assuming a lipid-based scatterer in a water-based medium. The curve labeled Muscle was the result of assuming an aqueous scatterer in the same water-based medium used for the lipid scatterer.

Straube et al, 1994, 2005

MR Thermometry

	PRF	Spectro-scopic	Diffusion	T1	Mo
Linear signal change with temperature	++	++	--	--	--
Valid from body temperature to >90°C	++	++	+/-	--	+/- (80°C)
Sensitivity	+/-	+/-	+	+/-	--
Ease of implementation	++	--	--	+/-	--
Tissue-type independent	++	++	---	---	+/-
Acquisition time	++	--	+/-	--	--

PRF Shift MR Thermometry

- Proton Resonant Frequency (PRF) Shift
- Based on the molecular structure of water and its dependence on temperature
- Water is a slightly polar molecule due to covalent bonds between oxygen & hydrogen
  - Causes attraction between neighbouring water molecules (Hydrogen bond)
  - Up to 4 hydrogen bonds/molecule

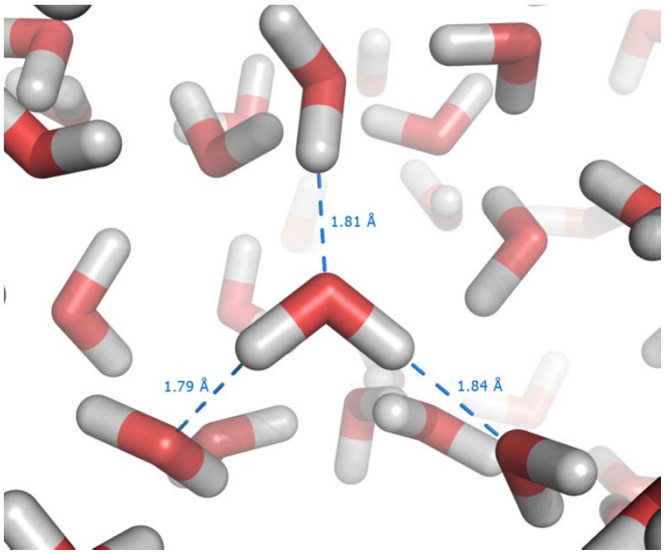

http://en.wikipedia.org/wiki/File:Liquid_water_hydrogen_bond.png

Table 4. Results of hydrogen bond analyses for liquid water at 1 atm†

	Temperature, °C				
	−25	0	25	60	100
No. of H-bonds	3·76	3·69	3·59	3·41	3·24
ε (H-bond)	−18·1	−17·8	−17·2	−17·0	−16·6
ε (Coulomb)	−24·4	−23·6	−22·8	−22·2	−21·4
ε (LJ)	6·3	5·9	5·6	5·1	4·7
θ, deg	161	159	157	156	154
φ, deg.	100	99	99	98	98
Percentage of monomers in *n* H-bonds					
n = 0	0·0	0·0	0·0	0·1	0·2
n = 1	0·3	0·4	0·9	1·8	3·2
n = 2	4·0	6·0	8·0	12·8	17·5
n = 3	25·2	28·8	33·3	35·9	38·3
n = 4	61·1	54·4	47·2	41·1	33·8
n = 5	9·0	9·8	10·0	7·9	6·5
n = 6	0·4	0·5	0·6	0·4	0·5

† εs in kJ mol^{-1}. ε (H-bond) is the average hydrogen bond energy which can be decomposed into Coulomb, ε (Coulomb), and Lennard-Jones, ε (LJ), terms. A hydrogen bond is defined by an interaction energy of −9·4 kJ mol^{-1} or less.

Jorgensen, Mol.Phys. 1985

PRF Shift MR Thermometry

- Change in hydrogen bond numbers changes the electron cloud shared between oxygen and hydrogen
- Local magnetic field experienced by protons affected by electron cloud

$$B_{loc} = (1-s)B_o$$

$$\omega = \gamma(1-s(T))B_o$$

- $s(T) = \alpha T$, $\alpha = 0.01 \times 10^{8}/°C$
- @1.5Tesla : 0.64 Hz/°C

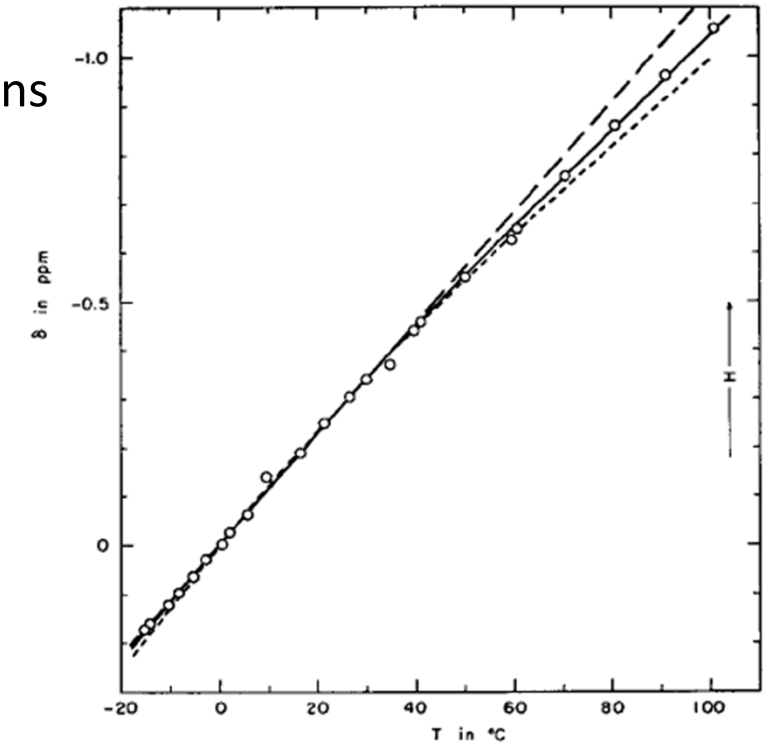

FIG. 1. Chemical shift of water as a function of temperature, δ_{H_2O} at 0°C=0. ○, Experimental data; —— straight line; – – – –, susceptibility corrected shift line.

Hindman, Chem Phys, 1966

PRF shift: Implementation

- ***Ishihara et al, Magnetic Resonance in Medicine, 34: 1995***
- Change in frequency results in change of phase in an MR image
- Phase changes in MR images caused by other factors as well
  - Motion, background field variations

$$\Delta B_o(T(\vec{r})) = B_{stat}(\vec{r}) + B_c(T(\vec{r}))$$

$$\phi(T(\vec{r})) = \gamma \cdot \Delta B_o(T(\vec{r})) \cdot TE$$

$$\phi(T(\vec{r})) - \phi(T_o(\vec{r})) = \Delta\phi = \gamma \cdot TE \cdot [\Delta B_o(T(\vec{r})) - \Delta B_o(T_o(\vec{r}))] = \gamma \cdot TE \cdot \Delta B_c(T(\vec{r}))$$

$$\Delta\phi(\vec{r}) = \gamma \cdot TE \cdot (\alpha B_o \cdot \Delta T(\vec{r}))$$

$$\Delta T(\vec{r}) = \frac{\Delta\phi(\vec{r})}{\gamma \cdot TE \cdot \alpha \cdot B_o}$$

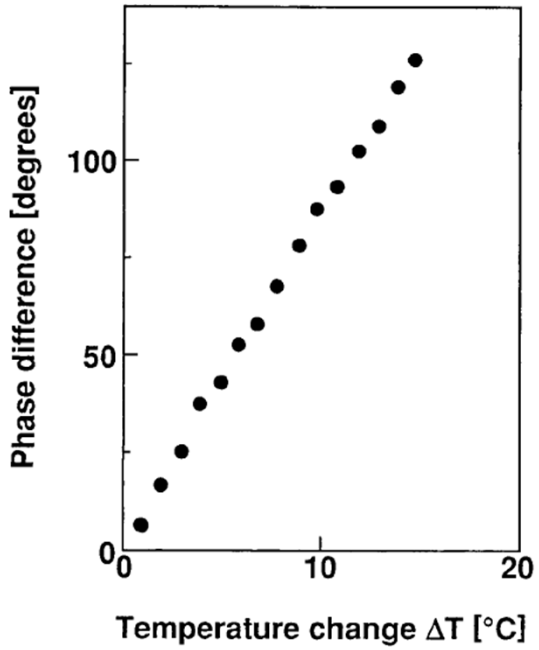

FIG. 4. Temperature dependence of the water proton chemical shift of a 1% NaCl solution. The temperature changes were measured with a thermocouple, and the phase differences were calculated from the average phase values surrounding the thermocouple.

PRF shift: Implementation

- Static field inhomogeneities always present in MRI, manifested as variations in phase image
- Subtraction of reference image (no heating) removes static field components

T(x,y)?

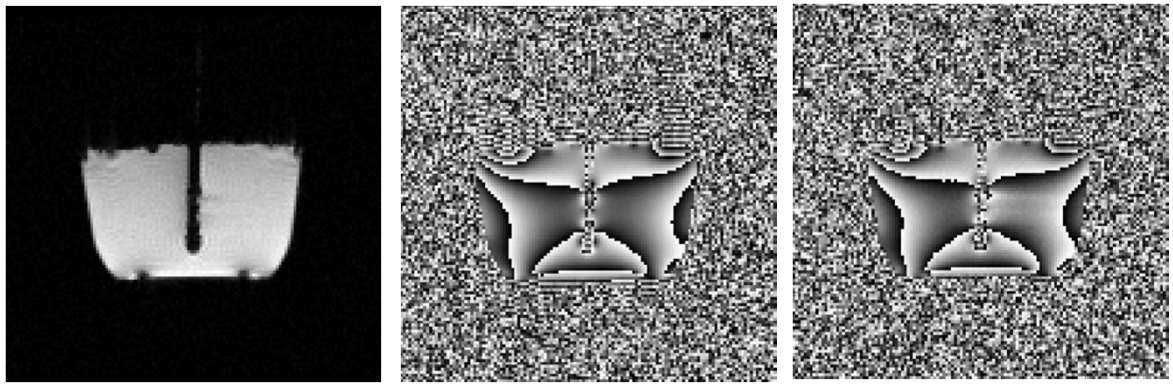

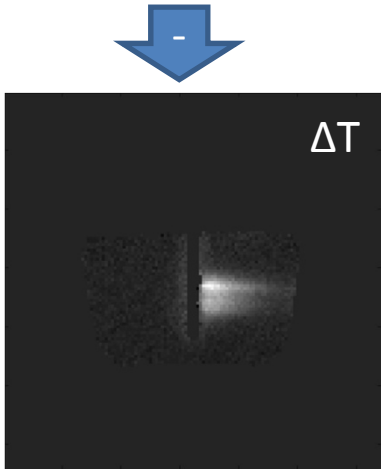

Correct For Baseline drift & Phase Wrap

$\Delta T_{corr} + T_{t_o} = T(x,y)$

PRF shift: Tissue-type independence

- ***Peters et al, Magnetic Resonance in Medicine, 40: 1998***
- Evaluated the PRF shift coefficient in a variety of tissue types (cooked and raw)

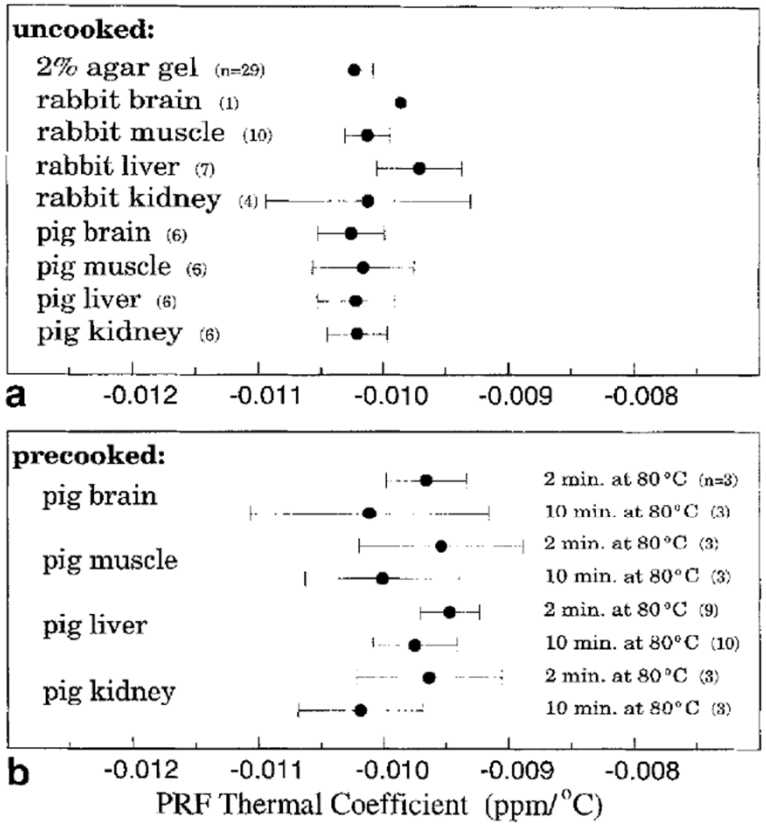

FIG. 7. PRF-thermal coefficients of (a) uncooked and (b) precooked *ex vivo* rabbit and pig tissues obtained from this particular experimental arrangement. The error bars indicate a 95% confidence interval for an estimate in the mean using the Student's *t* distribution. Only one data point was acquired for rabbit brain.

PRF shift: Sensitivity

- Very sensitive to displacements of objects in or around the imaging plane
  - Motion results in mis-registration of images
  - Susceptibility variations result in apparent temperature changes

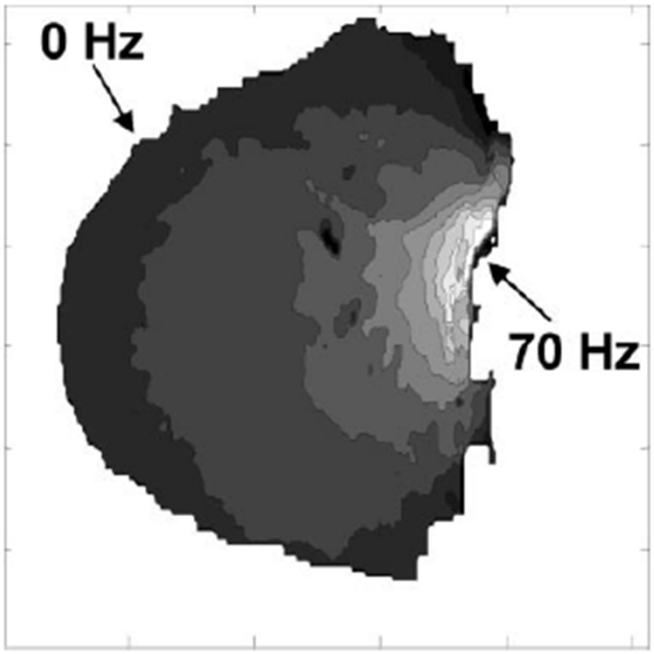

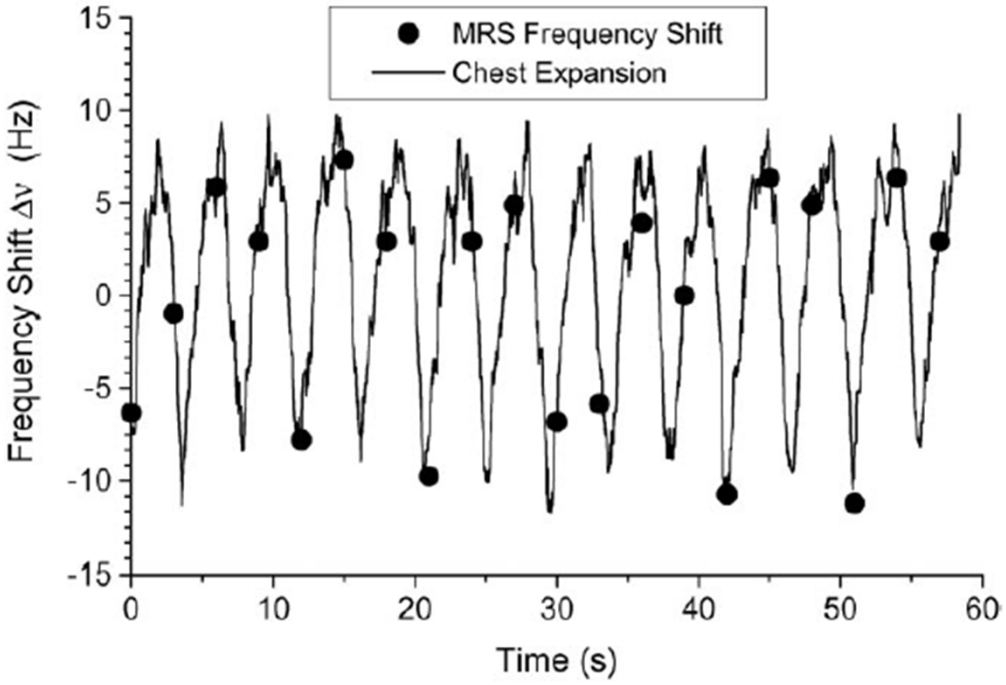

Equivalent to ± 6 °C in ROI due to breathing

Bolan et al, MRM, 2004

PRF shift: Validation

- Strong correlation with implanted temperature sensors

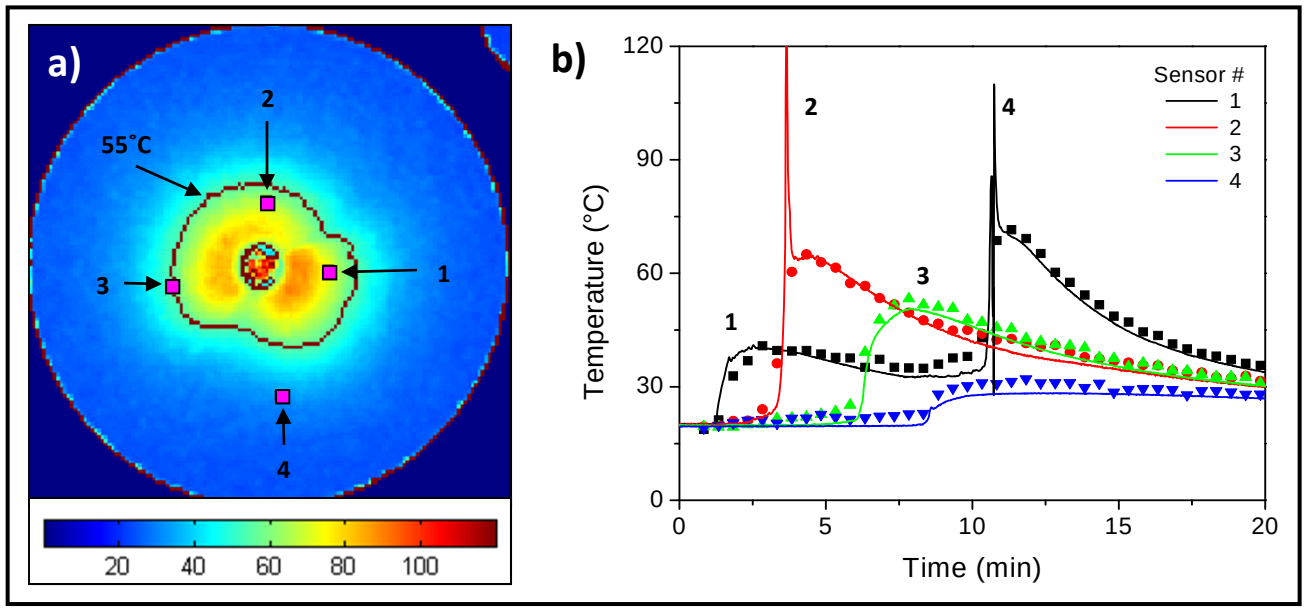

Figure 6: (a) Cumulative maximum temperature distribution measured for a prostate-simulating, 360º treatment in a tissue-mimicking gel showing the location of implanted temperature sensors. (b) Temperature measured as a function of time at each sensor during heating (solid lines) with the corresponding measurements made with MR thermometry (points).

Clinical Example

- MRI-guided focused ultrasound surgery of breast fiberadenoma (Hynynen et al, 2001)
- 9 patients treated prior to surgery

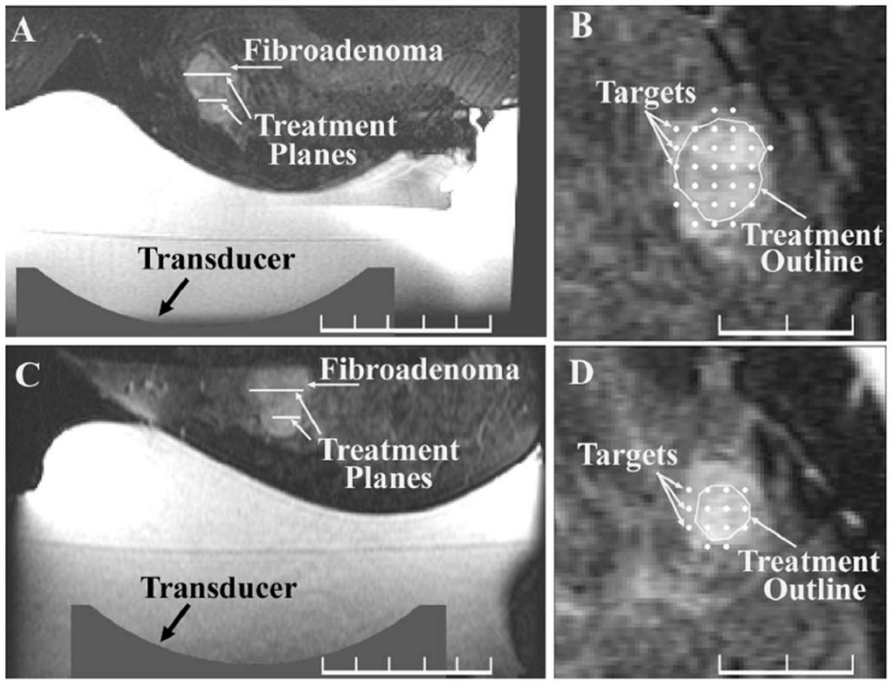

Figure 2. Fat-suppressed T2-weighted fast SE MR images (2,500/100) obtained for planning on the day of treatment of a fibroadenoma. The patient is lying in a prone position, with the breast positioned on the water pillow. The transducer is outlined at the bottom. Transverse sections (*A*, *C*) and the corresponding coronal sections (*B*, *D*) of the planning target volume outlined in two sequential planes are shown. The positions of the treatment foci are demonstrated in *B* and *D*.

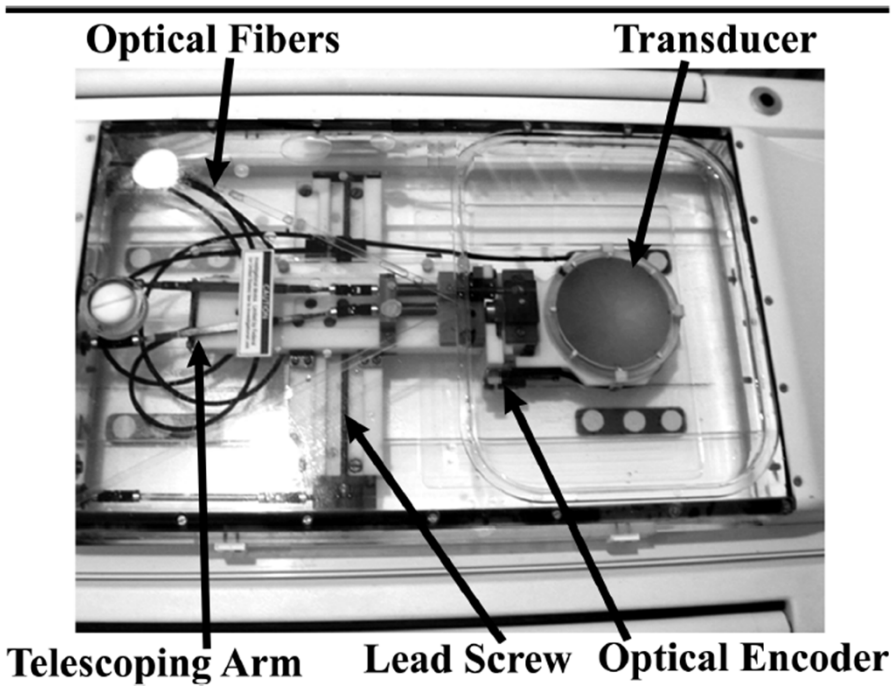

Clinical Example

- MRI-guided focused ultrasound surgery of breast tissue

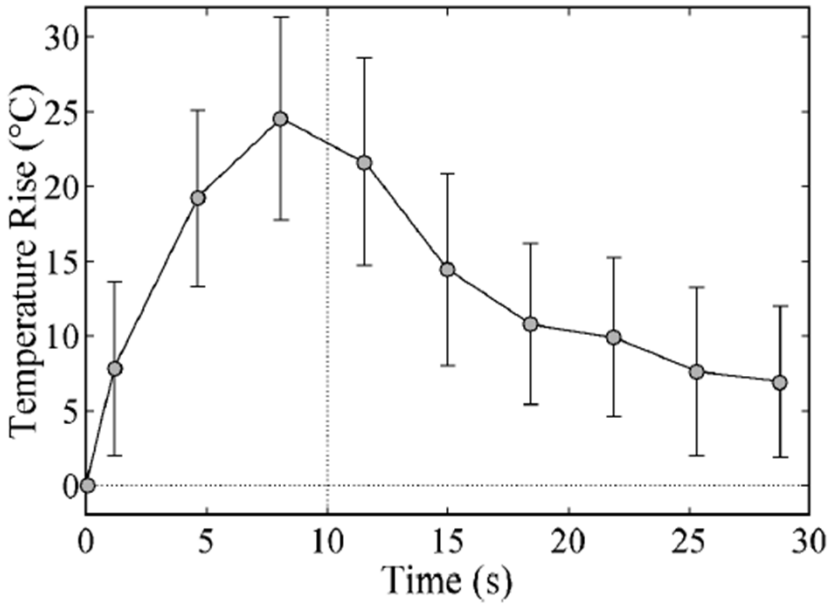

Figure 4. Graph shows mean temperature elevation as a function of time of the hottest voxel of 63 sonications delivered to a breast fibroadenoma, as measured with MR imaging–derived thermometry. The temperature increase was 17.5°–45.2°C. A total of 71 sonications in three planes were delivered to this tumor. Temperature increase could not be reliably monitored in eight sonications because of noise on the images, which was induced by fatty tissue surrounding the tumor.

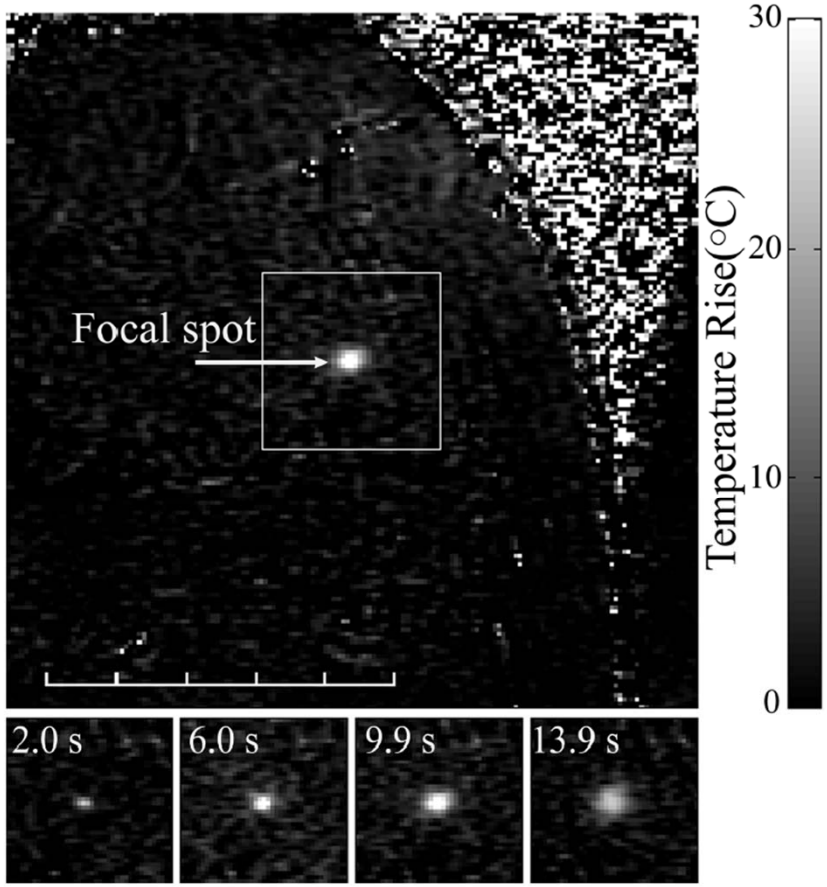

Figure 3. Temperature-sensitive fast spoiled gradient-echo phase-subtraction MR images (27.3/13.5) of a single 10-second therapeutic sonication in the tumor. Top: MR image shows the temperature elevation at the end of a sonication during therapy in the tumor in Figure 2, *A*, with proton resonance frequency imaging. The temperature focus appears as a small hyperintense spot in the breast. Bottom: MR images show the temperature time-course of the same sonication in the

Clinical Example

- MRI-guided focused ultrasound surgery of uterine fibroids (Tempany et al 2003)
- Nine patients underwent non-invasive thermal coagulation of a volume within an existing fibroid, prior to surgery
- Only a single plane was treated

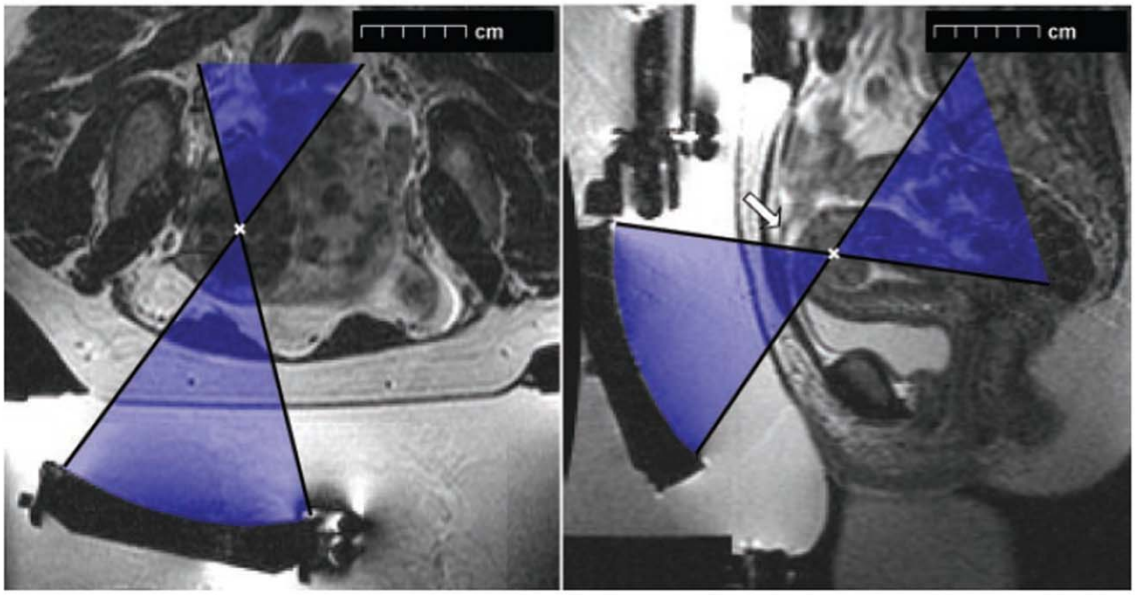

Figure 2. Patients 3 and 4. Transverse (left, patient 3) and sagittal (right, patient 4) T2-weighted fast SE MR images (2,500/98) with the patient in position for ultrasound surgery of uterine fibroids. In these cases, the transducer was angled during the treatment. The arrow on the right indicates the bowel loop that was avoided by angling the transducer.

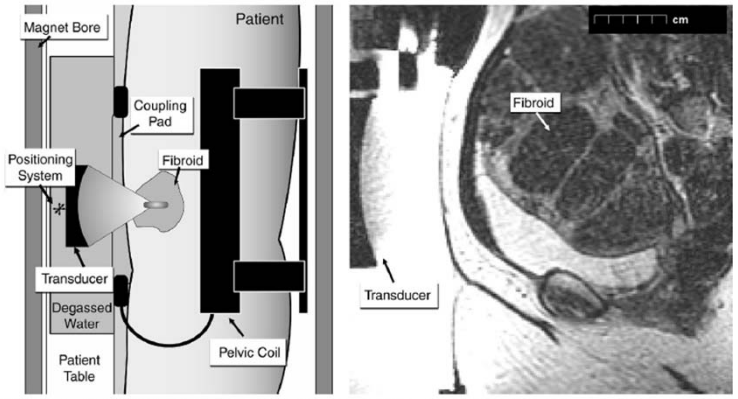

Figure 1. Patient 2. Left: Side-view diagram of the focused ultrasound system and patient positioning. Right: Sagittal T2-weighted fast SE MR image (repetition time msec/echo time msec = 2,500/98) obtained with the patient in position for treatment.

Clinical Example

Room time: 3h19 – 4h55

Treatment time: 1h – 2h32

Sonication time: 0.5 – 2h15

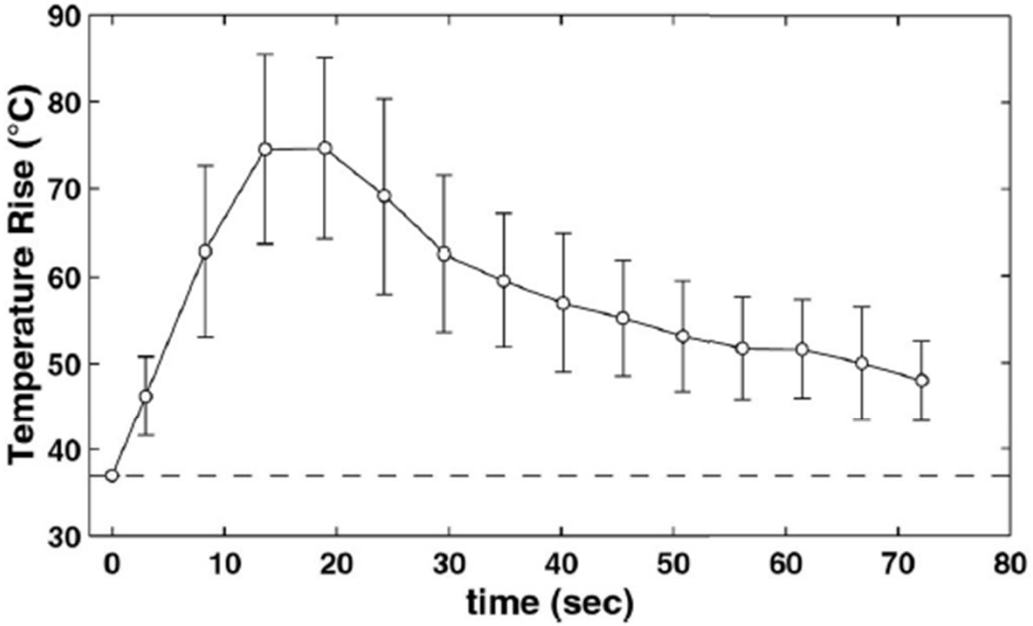

Figure 6. Patient 8. Line graph depicts temperature measured at the focus for 23 sonications in one treatment. The focal temperature increase was sufficient to cause thermal damage in each case. The variation from location to location was significant. Error bars = SD, dotted line = baseline body temperature (37°C).